

Effective transmittance of Fabry-Perot cavity under non-parallel beam incidence

Yin-Sheng Lv(吕寅生), Pin-Hua Xie(谢品华), Jin Xu(徐晋), You-Tao Li(李友涛), and Hua-Rong Zhang(张华荣)
Citation: Chin. Phys. B, 2024, 33 (**1**): 014210. DOI: 10.1088/1674-1056/ad0ec3
Journal homepage: http://cpb.iphy.ac.cn; http://iopscience.iop.org/cpb

What follows is a list of articles you may be interested in

Young's double slit interference with vortex source

Qilin Duan(段琦琳), Pengfei Zhao(赵鹏飞), Yuhang Yin(殷玉杭), and Huanyang Chen(陈焕阳)
Chin. Phys. B, 2024, 33 (**1**): 014202. DOI: 10.1088/1674-1056/acfdfd

Active control of surface plasmon polaritons with phase change materials

Yuan-Zhen Qi(漆元臻), Qiao Jiang(蒋瞧), Hong Xiang(向红), and De-Zhuan Han(韩德专)
Chin. Phys. B, 2023, 32 (**10**): 104202. DOI: 10.1088/1674-1056/accd5a

High-sensitivity methane monitoring based on quasi-fundamental mode matched continuous-wave cavity ring-down spectroscopy

Zhe Li(李哲), Shuang Yang(杨爽), Zhirong Zhang(张志荣), Hua Xia(夏滑), Tao Pang(庞涛),Bian Wu(吴边), Pengshuai Sun(孙鹏帅), Huadong Wang(王华东), and Runqing Yu(余润磬)
Chin. Phys. B, 2022, 31 (**9**): 094207. DOI: 10.1088/1674-1056/ac5d33

Design of three-dimensional imaging lidar optical system for large field of view scanning

Qing-Yan Li(李青岩), Yu Zhang(张雨), Shi-Yu Yan(闫诗雨),Bin Zhang(张斌), and Chun-Hui Wang(王春晖)
Chin. Phys. B, 2022, 31 (**7**): 074201. DOI: 10.1088/1674-1056/ac4a67

Relation between Airy beams and triple-cusp beams

Ren Zhi-Jun (任志君), Li Xiao-Dong (李晓东), Jin Hong-Zhen (金洪震), Chen Chen (陈晨), Wu Jiang-Miao (吴疆苗)
Chin. Phys. B, 2014, 23 (**8**): 084202. DOI: 10.1088/1674-1056/23/8/084202

Effective transmittance of Fabry–Perot cavity under non-parallel beam incidence

Yin-Sheng Lv(吕寅生)[1], Pin-Hua Xie(谢品华)[1,2,3,†], Jin Xu(徐晋)[2,‡], You-Tao Li(李友涛)[1], and Hua-Rong Zhang(张华荣)[2]

[1] *School of Environmental Science and Optoelectronic Technology, University of Science and Technology of China, Hefei* 230026, *China*
[2] *Key Laboratory of Environment Optics and Technology, Anhui Institute of Optics and Fine Mechanics, HFIPS, Chinese Academy of Sciences, Hefei* 230031, *China*
[3] *University of Chinese Academy of Sciences, Beijing* 100049, *China*

(Received 29 June 2023; revised manuscript received 9 October 2023; accepted manuscript online 22 November 2023)

The Fabry–Pérot (FP) resonant cavity is widely used in laser and spectroscopic measurements due to its unique interference transfer function (ITF). In the ideal case of parallel incident light, the ITF of the FP resonant cavity can be expressed by the Airy function. However, in reality, it is difficult to achieve perfect parallelism with collimated beams. In this article, a theoretical model is established for non-parallel light incidence, which assumes that the non-parallel incident light is a cone-shaped beam, and the cone angle is used to quantify the non-parallelism of the beam. The transmittance function of the FP resonant cavity under non-parallel light incidence is derived. The accuracy of the model is experimentally verified. Based on this model, the effects of divergence angle, tilt angle and FP cavity parameters (reflectivity, cavity length) on the ITF are studied. The reasons for the decrease in peak value, broadening and asymmetry of the interference peak under non-parallel light incidence are explained. It is suggested that a fine balance between the interference peak and the collimation effect of the incident light should be considered in the design and application of FP resonant cavities, especially for tilted applications such as angle-scanned spectroscopy. The research results of this article have certain significance for the design and application of FP resonant cavities.

Keywords: Fabry–Pérot (FP) resonant cavity, interference transfer function, Airy function, non-parallel beam incidence

PACS: 42.25.Hz, 42.79.–e, 42.15.Dp, 42.25.Bs **DOI:** 10.1088/1674-1056/ad0ec3

1. Introduction

A Fabry–Pérot (FP) cavity is typically composed of two parallel mirror surfaces, allowing multiple beam reflections and generating multi-beam interference.[1,2] FP cavity is widely utilized in various fields, such as precise interferometric measurements,[3] high-resolution spectroscopy[4–6] and fiber sensing,[7–9] due to its ability to increase the optical path length and its unique interference transfer function. Under ideal conditions, when a parallel beam is incident on the FP cavity, its interference transfer function can be accurately predicted by the Airy function.[10,11] However, in practical situations, achieving an ideal parallel beam is challenging, and the non-parallel incidence of the beam has a significant impact on precise spectroscopic measurements using FP cavities, particularly in applications where tilted beam incidence or spectral scanning through angle adjustment of the FP cavity is required. Therefore, considering the divergence angle of the beam is particularly important in understanding the influence on the interference transfer function of the FP cavity.

In previous studies, we utilized the angular dependence of the transmission spectrum structure of an FP etalon to achieve selective measurement of SO_2 gas by changing the angle of incidence.[5,6,12] However, further investigations revealed that when using higher-precision FP cavities, the interference transfer function (ITF) of the FP cavity is significantly affected by the beam divergence angle. Previous research by Vargas-Rodriguez *et al*. considered the variations in the ITF of the FP cavity when a focused beam is normally incident.[13] Marques *et al*. employed angular spectrum analysis to establish a model and studied the effects of mirror parallelism, planarity and the ITF for Gaussian beam focusing.[14–17] However, most of these studies focused on laser applications with small divergence angles and normal incidence.[18–20] There is relatively limited research on the general case of non-parallel beam incidence, particularly for large divergence angles and tilted beam incidence. Furthermore, investigating the impact of non-parallel beam incidence on the ITF for FP cavities with different physical parameters would be valuable. This research would contribute to better determining the appropriate FP cavity parameters for practical applications.

To quantitatively evaluate the impact of non-parallel incident beams on the ITF of FP cavities, this study established a geometric model and derived a formula for the ITF of FP resonant cavities when non-parallel beams are incident. In

†Corresponding author. E-mail: phxie@aiofm.ac.cn
‡Corresponding author. E-mail: jxu@aiofm.ac.cn

© 2024 Chinese Physical Society and IOP Publishing Ltd

this study, it was assumed that non-parallel beams have a certain divergence angle, and the positive and negative values of the divergence angle correspond to the convergence and divergence of the beams, respectively. The accuracy of the model was verified through experiments. Subsequently, the study quantitatively investigated the effects of the divergence angle and tilt angle on the interference transfer, and analyzed how the parameters of the resonant cavity, such as mirror reflectivity and cavity length, affect the ITF when the incident beam is non-parallel. The research in this study is significant for the design and precise measurement of FP interferometers.

2. Theory

In general, an FP resonant cavity consists of two mirrors placed parallel to each other, and the ITF of the resonant cavity is described by the Airy function. The basic form of the ITF is as follows:

$$T_{\mathrm{FP}} = \frac{(1-R_1)(1-R_2)}{(1-\sqrt{R_1R_2})^2 + 4\sqrt{R_1R_2}\sin^2(\phi)}, \tag{1}$$

where R_1 and R_2 are the reflectivities of the two mirrors that form the FP resonant cavity. Without considering factors such as absorption in the mirror coatings, the theoretical peak value of the ITF of the FP cavity is given by

$$T_{\mathrm{FP}}^{\mathrm{peak}} = \frac{(1-R_1)(1-R_2)}{(1-\sqrt{R_1R_2})^2}. \tag{2}$$

In most cases, the FP cavity is made up of two mirrors with the same reflectivity. When the reflectivities are the same, the interference peak has a theoretical peak transmittance of 100% (without considering absorption and scattering effects). Differences in mirror reflectivities will directly lead to a reduction in the peak transmittance of the ITF of the FP resonant cavity. In this study, we assume that $R_1 = R_2 = R$.

In Eq. (1), φ represents the phase difference between two successive light beams emitted from the resonant cavity. For the case of parallel light incidence, the phase difference between two successive light beams emitted from the resonant cavity is $\phi = 2\pi nd\cos\alpha/\lambda$, where n represents the refractive index of the medium inside the resonant cavity, d is the cavity length, λ is the wavelength of the incident light, and α represents the propagation direction of light inside the resonant cavity, which is the inclined angle between the incident light and the normal to the FP cavity. The FP resonant cavity with a fixed refractive index n and cavity length d is called the FP etalon sample. The Airy distribution function in Eq. (1) can be rewritten as

$$T_{\mathrm{FP}}(R,n,d,\lambda,\alpha) = \frac{1}{1+\dfrac{4R}{(1-R)^2}\sin^2\left(\dfrac{2\pi nd\cos\alpha}{\lambda}\right)}. \tag{3}$$

The finesse coefficient F is usually defined as $F = 4R/(1-R)^2$. The finesse of an FP resonator is affected by the mirror reflectivity R, with a higher reflectivity resulting in more interfering light in the resonator and a sharper interference peak in the resonator's ITF.

2.1. Theoretical model

The theoretical ITF of the FP cavity in Eq. (3) can only be directly used for parallel light incidence, as shown in Fig. 1(a). However, in practical situations, it is difficult to achieve perfect parallel incidence of the beam passing through the FP cavity, and the incident beam will always have some convergence (Fig. 1(b)) or divergence (Fig. 1(c)). Here, we assume that the beam enters the FP resonant cavity at a cone angle and quantify the non-parallelism of the beam with the size of the incident half-cone angle θ. When the beam converges, θ is positive, and when the beam diverges, θ is negative. We assume that the beam is entirely contained within a cone with a maximum divergence angle of $\theta_{\max}$. When the tilt angle between the cone axis and the normal of the FP cavity is α, as shown in Fig. 1(d), the transmission function of the beam passing through the FP cavity can be calculated. The FP cavity ITF in Eq. (3) still applies to beams at any angle. At this time, the actual cone angle θ of the beam in the cone and the rotation angle φ along the incident cone axis can be calculated for the actual incident angle γ of any light ray in the incident cone, using the geometric relationship shown in Fig. 1(d), with the cone tilt angle α:

$$\gamma = \arccos(\cos\alpha\cos\theta + \sin\alpha\sin\theta\cos\varphi). \tag{4}$$

Therefore, for all incident beams within the entire cone angle of the beam, it can be considered as any incident beam within the cone angle of the beam, and its incident tilt angle within the cone angle is γ. The transfer function of the beam can be obtained by integrating within the cone range (polar angle $\theta \in [0,\theta_{\max}]$, azimuth angle $\varphi \in [0,2\pi]$), which gives the FP cavity ITF when the non-parallel beam is normally incident:

$$\begin{aligned} &T_{\mathrm{FP}}(R,n,d,\lambda,\gamma,\theta_{\max}) \\ &= \frac{1}{N}\cdot\int_0^{2\pi}\int_0^{\theta_{\max}} \frac{\sin\theta\cos\theta}{1+F\sin^2\left(\dfrac{2\pi dn\cos\gamma}{\lambda}\right)}\,\mathrm{d}\theta\,\mathrm{d}\varphi, \end{aligned} \tag{5}$$

where $N = \int_0^{2\pi}\int_0^{\theta_{\max}}\sin\theta\cos\theta\,\mathrm{d}\theta\,\mathrm{d}\varphi$ is a normalization factor. Here, we present the FP cavity ITF function when the incident beam has a divergence angle. This formula includes both cases of beam convergence and divergence. The formula is an even function of the divergence angle θ, which means that the same ITF is generated for converging and diverging beams with the same divergence angle.

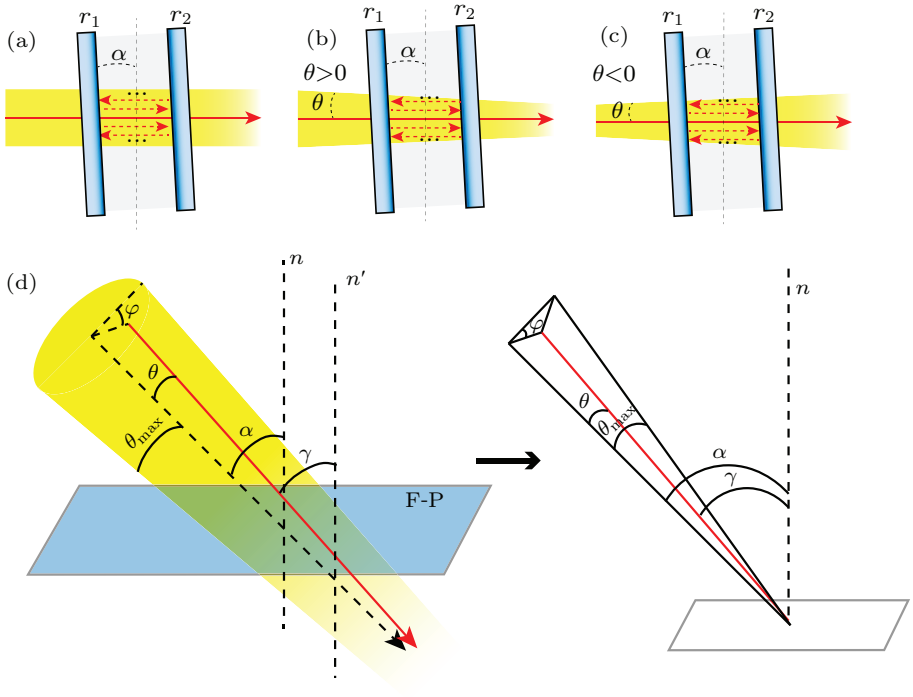


Fig. 1. (a) Parallel light incident on an FP cavity; (b) converging beam incident on an FP cavity, with a divergent angle $\theta > 0$ and a tilt angle α; (c) diverging beam incident on an FP cavity, with a divergent angle $\theta < 0$ and a tilt angle α; (d) non-parallel beam obliquely incident model. θ_{max} is the maximum divergent half-cone angle, α is the tilt angle, γ is the angle between any beam inside the cone and the normal of the FP cavity, θ is the polar angle and φ is the azimuthal angle.

2.2. Model verification

To validate the accuracy of the model for simulating FP cavities with non-parallel beam incidence, we designed an experimental setup, as shown in Fig. 2(a). The setup includes a custom FP etalon with a cavity length of 0.513 mm and an inner surface reflectivity of 95% in the 1600–1700 nm wavelength range. We used a tunable laser (Santec TSL-550) to perform continuous wavelength scanning in the 1598–1610 nm range to measure the ITF of the FP cavity. The laser output, which had a maximum divergence angle of about 0.03° after collimation, was used to simulate the theoretical calculation results with a maximum divergence angle of 0.03°. A laser power meter (VEGA PD300-IR) was used to receive the entire laser spot behind the FP etalon. To change the incident angle of the beam, we placed the FP etalon on a rotating stage and adjusted the tilt angle of the FP etalon by rotating the stage. The experimental results are shown in Figs. 2(b) and 2(c).

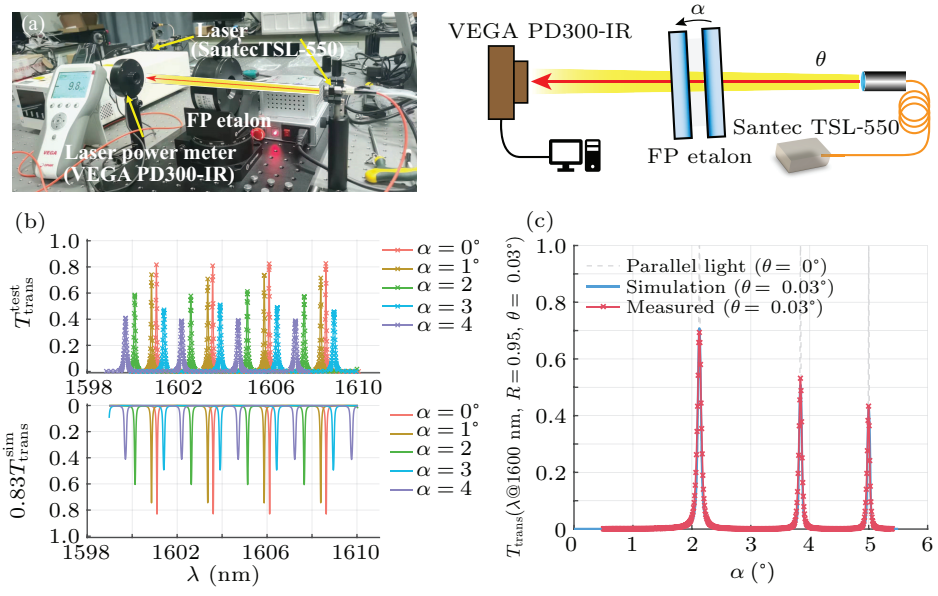


Fig. 2. (a) Experimental setup; (b) test transmittance (upper graph) and model simulation results (lower graph) of FP cavity at tilt angles of 0°, 1°, 2°, 3° and 4°; (c) test and simulation results of the transmittance of the FP cavity at 1600 nm as the tilt angle increases.

Figure 2(b) shows the measured and simulated results obtained by scanning the wavelength continuously from 1600 nm to 1610 nm and changing the tilt angle of the FP etalon to 0°, 1°, 2°, 3° and 4°. The upper figure shows the measured results, while the lower figure shows the simulated results. Both show good agreement with each other, with a system error of about 17%, possibly due to the influence of membrane absorption and scattering. Figure 2(c) shows the measured results of the transmittance, with the laser output wavelength fixed at 1600 nm and the tilt angle of the FP etalon changed continuously. These results are consistent with the model calculation results. The experiment demonstrates that the model we have established can accurately simulate the case of non-parallel beam incidence in FP cavities.

3. Results and discussion

This study, based on theoretical model calculations, discusses the influence of divergence angle, tilt angle and FP cavity standard parameters (reflectance, cavity length) on the ITF in an FP cavity system composed of two plane mirrors filled with air media with a refractive index of 1. The FP etalon has a fixed cavity length of 0.5 mm and the mirrors are coated with a reflective film with a reflectivity of 0.95 in the range of 1600–1700 nm, without considering the effects of absorption and scattering extinction of the film. We assume that the aperture of the FP cavity is much larger than the cross-sectional diameter of the beam passing through the FP cavity, and that the detector completely receives the light intensity at the detection end. We specifically focus on the case of non-parallel beam incidence.

To compare the changes in the effective transmittance of the FP cavity with parameter variations, we define visibility, sensitivity and trueness as follows:

$$\text{visibility} = \max(T_{\text{peak}}), \tag{6}$$

$$\text{sensitivity} = \frac{\text{visibility}}{\text{FWHM}}, \tag{7}$$

$$\text{trueness} = \lambda_{\text{peak}} - \lambda_0. \tag{8}$$

The visibility is defined as the maximum peak transmittance of the interference fringe. The sensitivity is defined as the ratio of visibility to the full width at half maximum (FWHM) of the peak, with higher sensitivity indicating a sharper interference fringe. The trueness is defined as the difference between the wavelength of the interference fringe and the theoretical peak position for parallel light incidence. A negative trueness indicates a shift of the interference fringe towards shorter wavelengths, while a positive trueness indicates a shift towards longer wavelengths.

3.1. The effect of divergence angle

To analyze the effect of non-parallelism of the incident beam on the FP cavity's ITF, we quantify the non-parallelism of the incident beam with the cone angle θ. Assuming the incident beam is normal to the FP cavity ($\alpha = 0°$), simulation results, as shown in Fig. 3, indicate that $\theta = 0$ corresponds to the case of parallel light incidence, where the theoretical peak transmittance of the ITF is 1 and the interference peak is the narrowest. As the cone angle of the incident beam increases, it can be observed from Figs. 3(a) and 3(b) that the transmittance of the FP cavity shows three trends: (i) the peak transmittance decreases, as shown in Fig. 3(c); (ii) the interference peak widens, as shown in Fig. 3(d); and (iii) the interference peak gradually shifts towards the short-wavelength direction. Meanwhile, under normal incidence, the interference peak is symmetrical in shape.

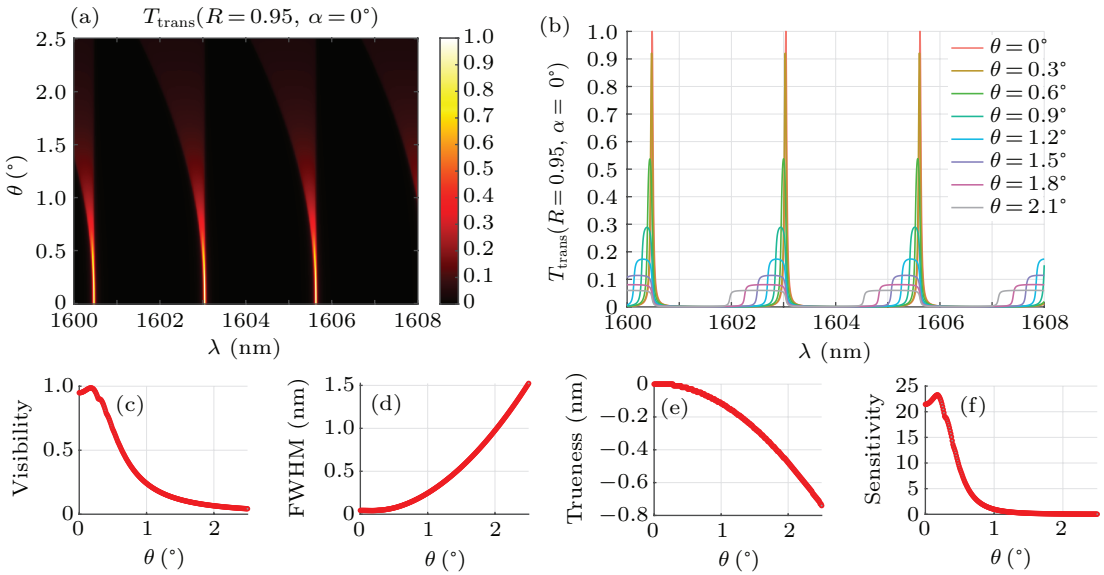


Fig. 3. (a), (b) Changes in FP transmittance with increasing divergent angle; (c) decrease in visibility with increasing divergent angle; (d) increase in the full width at half maximum of the interference peak with increasing divergent angle; (e) shift of trueness towards shorter wavelengths with increasing divergent angle; (f) decrease in sensitivity with increasing divergent angle.

The condition for the beam to resonate inside the FP cavity is that the optical path of the beam circulating in the cavity is an integer multiple of the wavelength,

$$2nd\cos\theta = m\lambda, \tag{9}$$

where m is an integer that represents the order of multiple-beam interference. The resonance wavelengths corresponding to the same interference order are associated with the propagation direction of the beam inside the FP resonant cavity. Therefore, the FP cavity is understood to be an angular spectral filter.[15] When there is a divergence angle, the propagation direction of the beam inside the FP cavity is no longer the same θ. For the case of parallel incidence with a cone angle $\theta_{\max}$, the beams entering the FP cavity include all propagation directions within the angle range of 0 to $\theta_{\max}$. Interference of the same order occurs at multiple resonance wavelengths, resulting in broadening of the interference peak. As the cone angle increases, the proportion of beams with the same propagation direction in the cone angle decreases, leading to a decrease in the interference peak value. At the same time, with the increase of the cone angle, the wavelength corresponding to the same interference order decreases, causing the interference peak to shift towards shorter wavelengths. Since the propagation direction of the incident beam is aligned with the normal direction of the FP cavity when parallel incidence occurs, the beams inside the cone angle are symmetrically distributed with respect to the normal direction of the FP cavity, resulting in a symmetric interference peak shape.

3.2. The effect of tilt angle

The effect of the tilt angle on the ITF of the FP cavity for non-parallel, oblique incident beams has been demonstrated in model validation experiments. The results show that with increasing tilt angle and the presence of beam divergence, the peak value of the FP interference fringes gradually decreases while the fringes become wider. Here, we further simulate the trend of the ITF as a function of the tilt angle at the same divergence angle ($\theta = 0.3°$), as shown in Fig. 4(a). With increasing tilt angle, the FP interference peak value decreases, the fringes become wider, and they shift towards shorter wavelengths. Figure 4(b) shows the trend of the angular transmittance function of the FP cavity at the same wavelength (λ@1600 nm) with increasing divergence angle, revealing that the position of the interference peak remains basically unchanged while the angular range widens and the peak value decreases as the divergence angle increases. Figure 4(c) shows the trend of a single interference peak as a function of the divergence angle at a tilt angle of $\alpha = 1°$. With increasing divergence angle, at the same tilt angle, the peak value of the interference fringes decreases, the width increases and the interference peak shape is no longer symmetric.

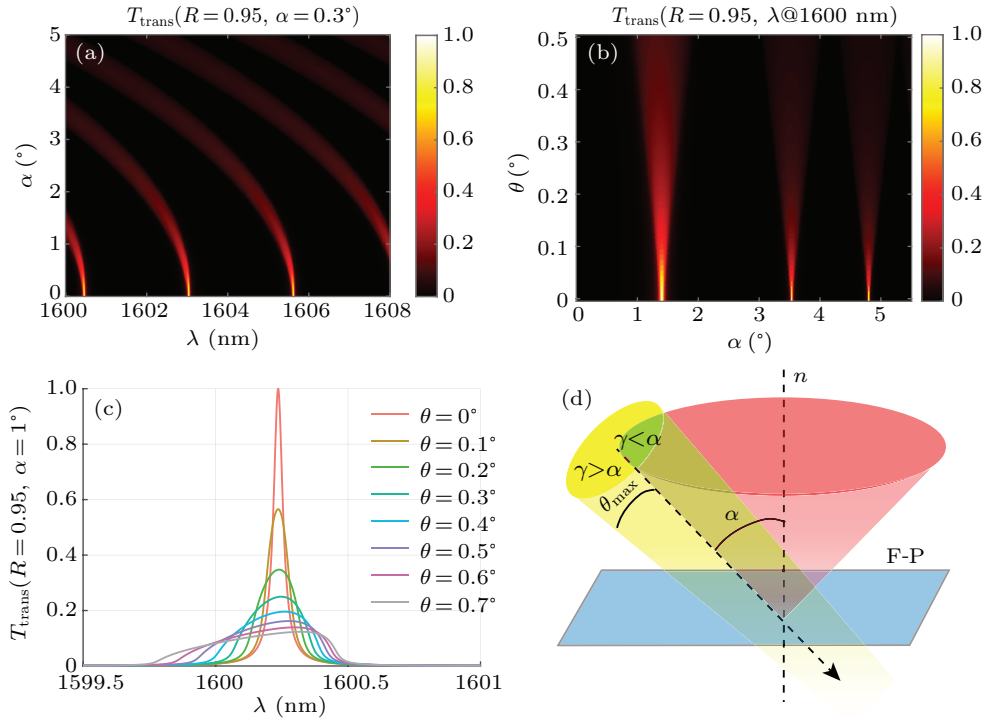


Fig. 4. The influence of tilt angle on the ITF of the FP cavity when non-parallel beams are incident. (a) Changes in the ITF of the FP cavity with increasing tilt angle at a divergent angle of $\theta = 0.3°$; (b) trend of angle-scanned transmittance at 1600 nm with increasing divergent angle; (c) curve of a single interference peak with varying divergent angle at a tilt angle of $\alpha = 1°$; (d) schematic diagram of a beam with a maximum divergent cone angle of $\theta_{\max}$ obliquely incident with a tilt angle of α, where the yellow region represents the actual incident angle $\gamma > \alpha$, the green region represents the actual incident angle $\gamma < \alpha$ and the red region represents the area where the maximum tilt angle with the FP normal as the axis is α.

For oblique incidence, when a beam with a maximum divergence angle of θ_{max} enters the FP cavity at an oblique angle α, as shown in Fig. 4(d), the actual incident angle γ of any light ray within the beam cone is within the angular range of

$$\gamma \in [\alpha - \theta_{max}, \alpha + \theta_{max}]. \tag{10}$$

The yellow region in Fig. 4(d) represents the area where the incident angle $\gamma > \alpha$, and the green region represents the area where $\gamma < \alpha$. The polar angle of the axis of the beam cone is denoted by θ_{max}. According to Eq. (9), for the same interference order, as the tilt angle α increases, the interference peak wavelength position shifts towards shorter wavelengths. When there is a divergence angle, the maximum width of the interference peak for the same interference order is given by

$$\begin{aligned} \Delta\lambda &= \left| \frac{2nd(\cos\gamma_{min} - \cos\gamma_{max})}{m} \right| \\ &= \frac{2nd}{m} |(\cos(\alpha - \theta_{max}) - \cos(\alpha + \theta_{max}))| \\ &= \frac{4nd \sin\alpha \sin\theta_{max}}{m}. \end{aligned} \tag{11}$$

Therefore, both an increase in the tilt angle α and an increase in the maximum divergence angle θ_{max} of the incident beam in oblique incidence will lead to broadening of the interference peak. The asymmetry of the interference peak broadening can be attributed to the inconsistency between the regions where the actual incidence angle γ is greater than α and where it is less than α. Specifically, an actual incidence angle γ greater than α will cause the resonant wavelength position to shift towards shorter wavelengths, while γ less than α will cause the resonant wavelength to shift towards longer wavelengths. When the energy of the beam is symmetrically distributed in the cone section, the proportion of the region where the actual incidence angle γ is greater than α is always larger than that where γ is less than α in oblique incidence. This will result in greater broadening towards shorter wavelengths than towards longer wavelengths on the interference peak, leading to asymmetry in the shape of the interference peak.

3.3. The effect of FP cavity reflectivity

Next, we further analyze the effect of the FP cavity's mirror reflectivity on ITF when non-parallel beams are incident on the FP cavity. Figure 5(a) shows the ITF curves for a beam

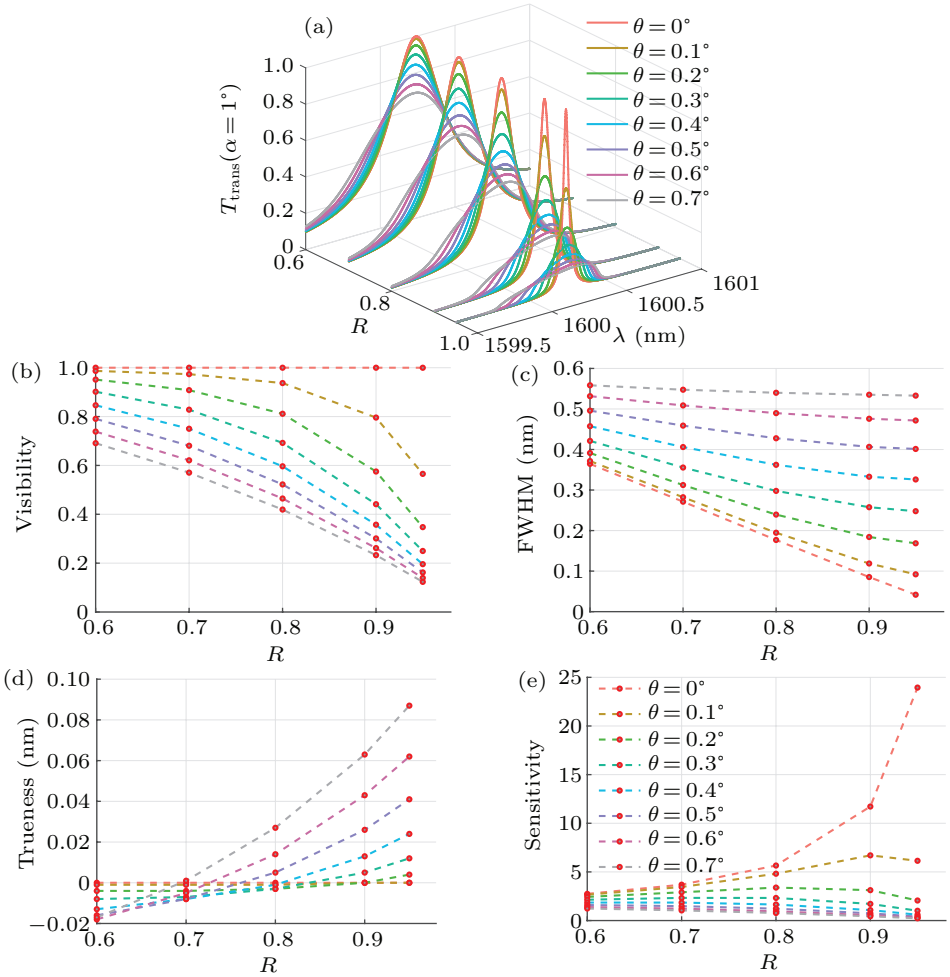


Fig. 5. The influence of FP cavity reflectivity on ITF. (a) The curve of FP interference fringe changing with divergent angle for different reflectivity values of 0.6, 0.7, 0.8, 0.9, 0.95; (b) the change of visibility with FP cavity reflectivity for different divergent angles; (c) the change of the full width at half maximum with FP cavity reflectivity for different divergent angles; (d) the change of trueness with FP cavity reflectivity for different divergent angles; (e) the change of sensitivity with FP cavity reflectivity for different divergent angles.

with a tilt angle of $\alpha = 1^\circ$ and with divergence angles of 0°, 0.1°, 0.2°, 0.3°, 0.4°, 0.5°, 0.6° and 0.7°, respectively, when the mirror reflectivity R of the FP cavity is 0.6, 0.7, 0.8, 0.9 and 0.95. As shown in Fig. 5(b), as the mirror reflectivity R increases, the visibility of the interference fringes of the FP cavity decreases for the same divergence angle of the incident beam. Figure 5(c) shows that for an FP cavity with low mirror reflectivity, the interference fringe position is less affected by the divergence angle compared to the high mirror reflectivity case. Figure 5(d) shows that the sensitivity first increases and then decreases with increasing reflectivity when there is a divergence angle. Moreover, for low mirror reflectivity, the visibility, full width at half maximum, trueness and sensitivity are less affected by the divergence angle compared to high mirror reflectivity.

The higher the mirror reflectivity of the FP cavity, the more light beams undergo interference inside the resonant cavity, resulting in higher finesse and narrower interference peak width. However, when the incident light has a divergence angle, the peak transmittance decreases more significantly, and reducing the reflectivity can provide higher peak transmittance for non-parallel incident beams at the cost of increased interference width. Therefore, for high-finesse FP resonant cavities (high mirror reflectivity), the incident beam divergence angle has a greater impact on the ITF. This suggests that if there are certain requirements for the peak transmittance and interference peak position of the FP ITF under non-parallel beam incidence, the mirror reflectivity of the FP cavity can be appropriately reduced to sacrifice some finesse and obtain greater tolerance for non-parallel incident beams.

3.4. The effect of FP cavity length

Changes in the cavity length of the FP cavity directly affect the resonant frequency of the cavity. In order to ensure that the interference peak is at the same wavelength position, we simulated the case where the cavity length is increased by integer multiples. In this case, the interference order corresponding to the same interference wavelength position increases by the same multiple. Figure 6 shows the ITF curve as a function of the divergence angle for cavity lengths of 0.5 mm, 1 mm, 2 mm and 4 mm. In Figs. 6(c) and (d), more interference peaks appear in the same wavelength range, which is due to the decrease in the free spectral range (FSR) of the FP cavity with increasing interference order,

$$\mathrm{FSR} = \frac{2nd\cos\alpha}{m(m+1)} \approx \frac{2nd\cos\alpha}{m^2}. \tag{12}$$

When the FP cavity length d increases by a factor of k, according to Eq. (9), the interference order corresponding to the same interference wavelength position increases by a factor of k. Then, the FSR changes as follows:

$$\mathrm{FSR}' = \frac{2nkd\cos\alpha}{km(km+1)} \approx \frac{2nd\cos\alpha}{km^2}. \tag{13}$$

Therefore, we can conclude that when the FP cavity length increases by an integer multiple, the FSR decreases at the same rate for high-order interference.

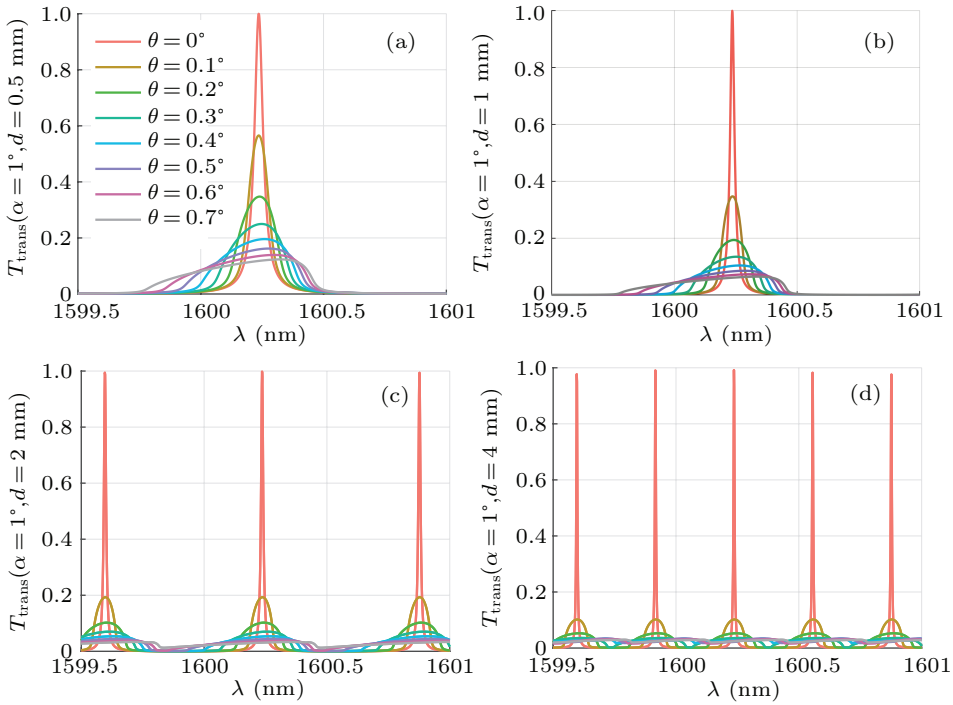


Fig. 6. The influence of FP cavity length on the ITF when non-parallel beams with a tilt angle of $\alpha = 1^\circ$ are obliquely incident. (a) The ITF varies with the divergence angle for a cavity length of $d = 0.5$ mm; (b) the ITF varies with the divergence angle for a cavity length of $d = 1$ mm; (c) the ITF varies with the divergence angle for a cavity length of $d = 2$ mm; (d) the ITF varies with the divergence angle for a cavity length of $d = 4$ mm.

In this discussion, we focus on a single interference peak at the same interference wavelength position. Figure 7(a) shows that with the same tilt angle of $\alpha = 1°$, the longer FP cavity has a significantly lower ITF as the divergent cone angle increases. The FWHM of the interference peak, shown in Fig. 7(b), decreases with increasing cavity length at lower divergent angles ($\theta < 0.2°$), mainly due to the increase in interference order. However, when the divergent angle is greater than 0.2°, the trend of decreasing FWHM with increasing cavity length is no longer obvious, and the FWHM increases with increasing divergent angle. When the cavity length is 4 mm, as shown in Fig. 6(d), when the divergent angle increases to 0.7°, the interference peak width is close to FSR, and the interference peak becomes flat. As shown in Fig. 7(c), the trueness of the interference peak wavelength position for shorter FP cavities is less affected by the divergent angle of the beam. Figure 7(d) shows that in the presence of a divergent angle, an increase in cavity length reduces the sensitivity of the interference peak, except for parallel beam incidence. The change in cavity length corresponds to a change in FP interference order. The high spectral resolution of the FP cavity mainly comes from high-order interference, which is more susceptible to the influence of non-parallel incident beams. Therefore, in practical applications, a balance needs to be struck between the precision of high-order interference and the non-parallel incidence of the incident beam.

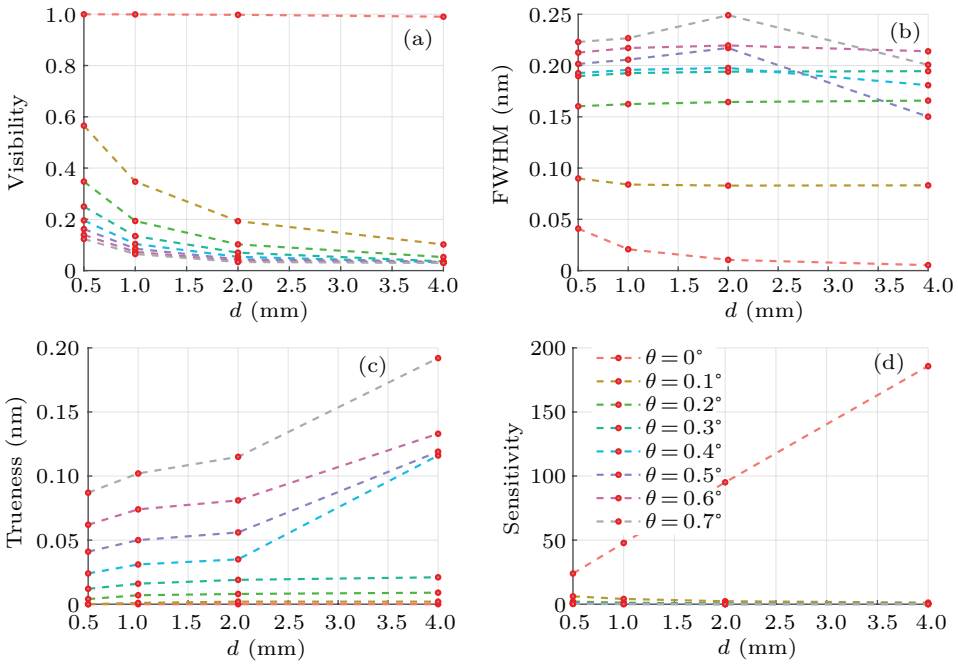


Fig. 7. (a) The visibility changes with the FP cavity reflectivity for different cavity lengths; (b) the FWHM changes with the FP cavity reflectivity for different cavity lengths; (c) the trueness changes with the FP cavity reflectivity for different cavity lengths; (d) the sensitivity changes with the FP cavity reflectivity for different cavity lengths.

4. Conclusion and perspectives

This study investigates the behavior of non-parallel light beams passing through an FP cavity ITF. The theoretical model is constructed assuming that the incident non-parallel light enters the FP cavity with a certain cone angle of divergence, and the transmission function with a certain cone angle of divergence is derived. An experiment is designed to verify the accuracy of the theoretical model by measuring the transmission function of a laser beam passing through an FP etalon with a known divergence angle under various laser wavelengths and FP tilt angles. The experimental results are in good agreement with the simulated results of the theoretical model. Based on the model, the effects of divergence angle, tilt angle and FP parameters (reflectivity, cavity length) on the ITF are analyzed. The results show that an increase in the divergence angle leads to a decrease in the ITF peak, broadening of the interference peak, and a shift towards the short wavelength direction. An increase in the tilt angle with a divergence angle present also leads to broadening of the interference peak and an asymmetric peak structure. Increasing the reflectivity of the FP cavity mirror can produce finer interference peak structures but is more susceptible to the non-parallel incident light. On the other hand, an increase in cavity length corresponds to an increase in interference orders, and the fine interference peak structures formed by high-order interference are also more susceptible to non-parallel incident light. In conclusion, when designing and using FP cavities (especially for FP cavity tilt applications, such as angle scanning spectroscopy), a balance between fine interference peaks and collimated incident light should be considered. Sacrificing some spectral resolution (such as reducing mirror reflectivity or cavity length, and lowering interference orders) often leads to greater tol-

erance to non-parallel incident light. This research on non-parallelism has significant implications for the design of FP cavities, such as MEMS-based FP micro spectrometers, and the precise measurement of FP cavities for applications such as spectral measurements based on FP angle scanning. Furthermore, based on the findings of this study, it may be possible to calculate the laser divergence angle by measuring the transmission of interference peaks using the FP cavity angle scanning method.

Acknowledgements

We gratefully acknowledge Mr Yingjie Ye for providing the laser used in the experiments.

Project supported by the National Natural Science Foundation of China (Grant No. U19A2044), the National Natural Science Foundation of China (Grant No. 41975037), and the Key Technologies Research and Development Program of Anhui Province (Grant No. 202004i07020013).

References

[1] Perot A and Fabry C 1899 *ApJ* **9** 87
[2] Treanor P J 1948 *Nature* **162** 885
[3] Bond C, Brown D, Freise A and Strain K A 2016 *Living Rev. Relativ.* **19** 3
[4] Shijun X and Weiner A M 2005 *IEEE Photonic Tech. Lett.* **17** 372
[5] Fuchs C, Kuhn J, Bobrowski N and Platt U 2021 *Atmos. Meas. Tech.* **14** 295
[6] Lv Y, Xie P, Xu J, Li A, Hu Z, Li Y, Zhang H, Zhang Z, Tian X, Hu F, Zheng J and Ye Y 2023 *Opt. Express* **31** 2602
[7] Kim H T, Hwang W, Liu Y and Yu M 2020 *Opt. Express* **28** 29937
[8] Quan M, Tian J and Yao Y 2015 *Opt. Lett.* **40** 4891
[9] Wang X D and Wolfbeis O S 2020 *Anal. Chem.* **92** 397
[10] Ismail N, Kores C C, Geskus D and Pollnau M 2016 *Opt. Express* **24** 16366
[11] Suter M and Dietiker P 2014 *Appl. Opt.* **53** 7004
[12] Kuhn J, Platt U, Bobrowski N and Wagner T 2019 *Atmos. Meas. Tech.* **12** 735
[13] Vargas-Rodrguez E and Rutt H N 2009 *Sensors and Actuators B: Chemical* **137** 410
[14] Marques D M, Guggenheim J A and Munro P R T 2021 *Opt. Express* **29** 24144
[15] Marques D M, Guggenheim J A and Munro P R T 2021 *Opt. Express* **29** 21603
[16] Marques D M, Guggenheim J A and Munro P R T 2022 *Opt. Express* **30** 46294
[17] Marques D M, Guggenheim J A, Ansari R, Zhang E Z, Beard P C and Munro P R T 2020 *Opt. Express* **28** 7691
[18] Lee J Y, Hahn J W and Lee H W 2002 *J. Opt. Soc. Am. A* **19** 973
[19] Xia G, Wu Z, Liu M and Pan Y 2003 *Optik* **114** 521
[20] Shen F, Wang Y, Shi W, Chen Y, Liu M and Guo W 2017 *LIDAR Imaging Detection and Target Recognition 2017* (SPIE) Vol. 10605